

Supporting Information

4-Electron redox enabled by a perylene diimide containing side-chain amines for efficient organic cathode

Zhiling He^a, Junfeng Zhu^a, Mingyu Yin^a, Deyi Liao^a, Jiajin Feng^b, Qingguang Zeng^b, Hui Yu^a, John H. Xin^c, Da Wang^{*b}, Xi Liu^{*a}

Experimental

Materials: All reagents were obtained from commercial sources and used without further purification. PDA, PDIN, and PDIC5 were purchased from J&K. Multi-walled carbon nanotubes (MWCNTs) were purchased from Shanghai McLean Biochemical Technology Co., Ltd. Poly vinylene difluoride (PVDF) was purchased from Beijing Huawei Ruike Chemical Co., Ltd.

Characterization: Fourier-transform infrared (FTIR) spectra data were collected with a Nicolet iS50 Fourier transform infrared spectrometer. XRD characterization was collected on a Rigaku SmartLab 9kW. Scanning electron microscopy (SEM) characterization was conducted using a Hitachi SU8200 instrument. X-ray photoelectron spectroscopy (XPS) characterization was conducted on Thermo Scientific Nexsa. The ex-situ FTIR was recorded on Bruker Alpha II FTIR Spectrometer using attenuated total reflectance (ATR) mode in the argon-filled glovebox. In-situ FTIR characterization was conducted using a FTIR spectrometer (Nicolet iS50, Thermo-Fisher Scientific) with an extended range silicon crystal ATR accessory. Cyclic voltammetry (CV) and electrochemical impedance spectroscopy (EIS) measurements were performed on an electrochemical workstation (CHI660E). Galvanostatic charge/discharge curves and rate capability tests were carried out on a Land test system (CT3001A, China).

Cathode fabrication, coin cell assembly and battery test: The organic positive electrode is composed of a mixture of 30% electroactive materials (PDA, PDIN, or PDIC5), 60% multi-walled carbon nanotubes (MWCNTs), and 10% poly vinylene difluoride (PVDF) binder. The mixing process was conducted using a conventional mortar and pestle, during which the

electroactive materials, MWCNTs, and PVDF were added to the mortar in sequence and ground for 20 min. The mixture was poured into a tablet mold and pressed into small discs with a diameter of 12 mm. The electrodes were dried at 80 °C in a vacuum oven for over 8 h before assembling coin-type cells in an argon-filled glovebox. The coin cells were composed of PDA, PDIN or PDIC5 as the working electrode, lithium metal disc as the anode, glass fiber as the separator and lithium bis(trifluoromethanesulphonyl)imide (LiTFSI) in 1,3-dioxolane/1,2-dimethoxyethane (DOL/DME, 1:1 in volume, 1.0 M) as the electrolyte. Galvanostatic charge-discharge cycling tests were carried out on a Land test system (CT3001A, China) between 1.5 and 3.8 V at 25 °C.

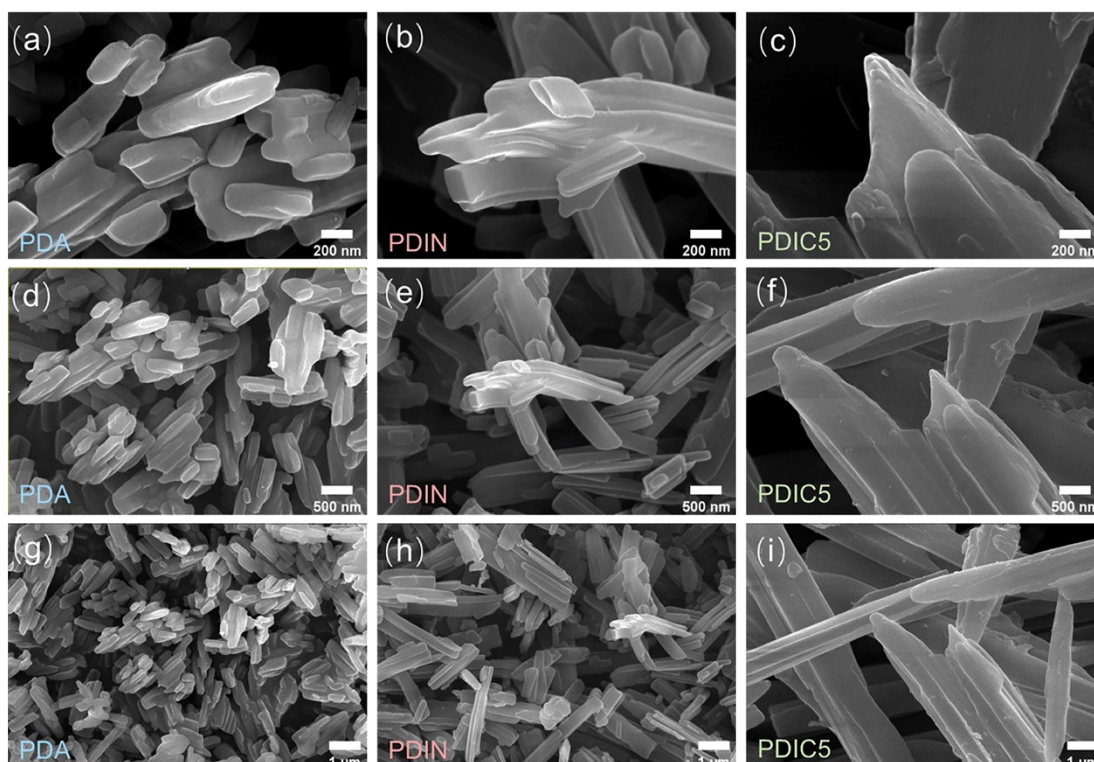


Fig. S1. SEM images of PDA (a, d, g), PDIN (b, e, h), and PDIC5 (c, f, i) powders under relevant scale bars.

The cycling stabilities of the batteries are shown in Figure S2a. PDIN-based battery showed a negligible capacity loss from 100 to 1000 cycles, maintaining a capacity of 100 mAh g⁻¹ after 1000 cycles. By contrast, PDA-based battery displayed a gradual and continuing capacity loss, resulting in a final capacity of only 55 mAh g⁻¹ after 1000 cycles. The PDIC5-based battery experienced a rapid and precipitous decline in cycling performance with a mere ~20% capacity remaining after only 20 cycles, indicative of its limited cycle life. Figure S2b presents the rate capabilities of the batteries. Compared to PDA and PDIC5, PDIN consistently exhibits high capacities and good rate performance. Meanwhile, the results of the charge storage mechanism and reaction kinetics analyses of these three cathodes (Figure S3-6) and the electrochemical impedance spectroscopy (EIS) measurements (Figure S7)

preliminarily suggest that PDIN exhibits high capacity, good stability, and good rate capability as a promising cathode material.

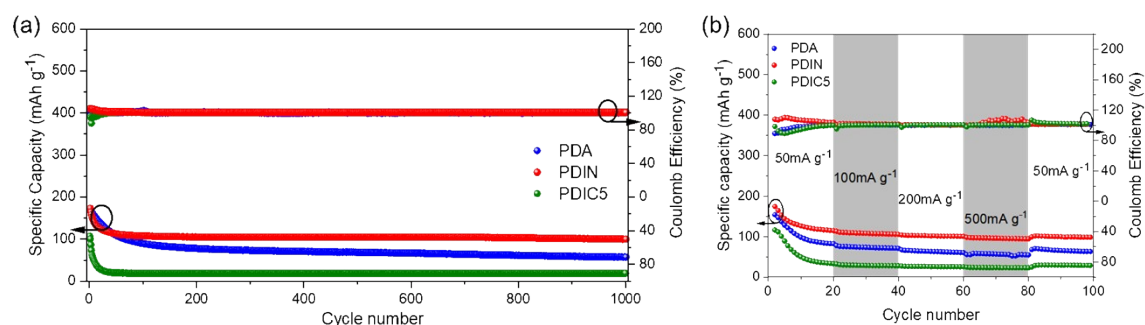


Fig. S2. (a) Cycling performance and Coulombic efficiency of the three molecules under a current rate of 500 mA g⁻¹ and (b) the rate capabilities of the batteries.

The charge storage mechanism and reaction kinetics of these three cathodes are investigated by CV measurements at different scan rates. The corresponding CV curves of the three batteries under increased scan rate from 0.1 to 0.5 mV s⁻¹ are shown in Figure S3a–c. Generally, the correlation of the peak current (*i*) and the scan rate (*v*) obeys the power law $i = av^b$, where a value of 0.5 for *b* indicates a diffusion control process, while a value of 1.0 for *b* implies a surface-controlled process.¹ Figure S3d–f shows the corresponding linear plots of logarithm oxidation (Peak A) and reduction (Peak B) peaks currents versus logarithm scan rates of PDA-, PDIN-, and PDIC5-based batteries, respectively. The *b*-values calculated from the approximate linearity of log(*i*) and log(*v*) of the oxidation peaks and reduction peaks of the three batteries. The Peak A/Peak B *b*-values of PDA-, PDIN-, and PDIC5-based batteries are 0.59/0.57, 0.64/0.71, and 0.24/0.33, respectively. The *b*-values results indicated that, compared to PDA and PDIC5, the PDIN-based cathode tends to be a mixed process of diffusion-controlled and surface-controlled charge-storage process. In addition, the capacitive contributions to the overall capacities of the cathodes at a certain scan rate were further calculated by the equation $i = k_1v + k_2v^{1/2}$, where *k*₁ and *k*₂ can be determined by plotting $iv^{-1/2}$ versus $v^{1/2}$ for linear simulation. The detailed results for these calculations of the three batteries are shown in Figures S4–S6. The corresponding capacitive contributions of the three batteries are consistent with their above *b*-values results. In particular, the PDIN-based battery showed high capacitance contributions at different scan rates and exhibited an increased capacitance contribution trend with the increase of scan rate, indicating its good rate performance.

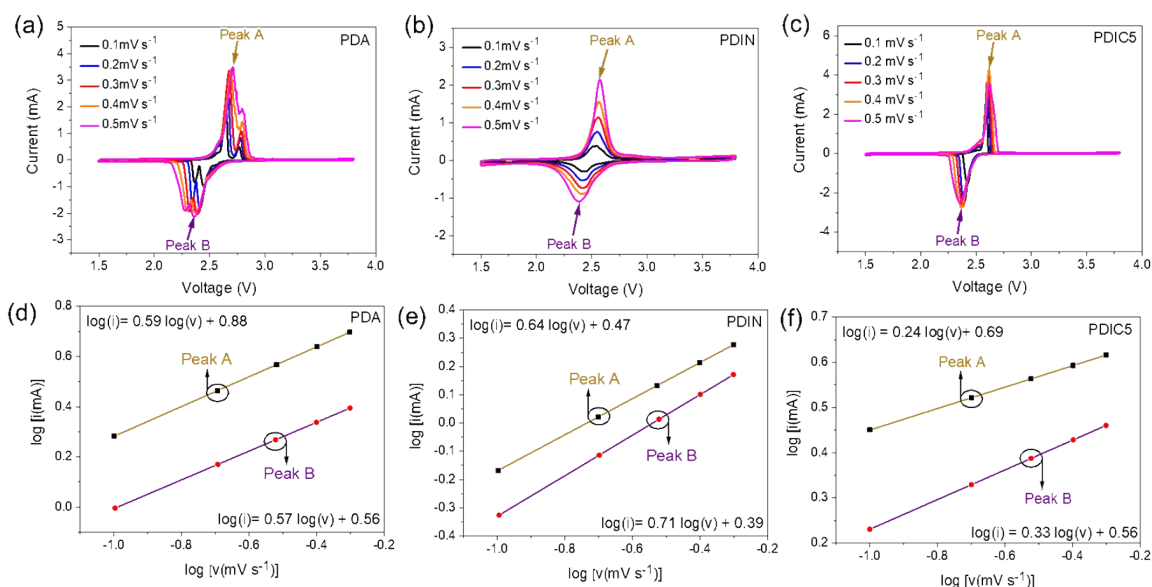


Fig. S3. CV curves of PDA- (a), PDIN- (b), and PDIC5- (c) based batteries, scan rate ranges from 0.1 to 0.5 mV s^{-1} ; the corresponding linear plots of logarithm oxidation (Peak A) and reduction (Peak B) peaks currents versus logarithm scan rates of PDA- (d), PDIN- (e), and PDIC5- (f) based batteries.

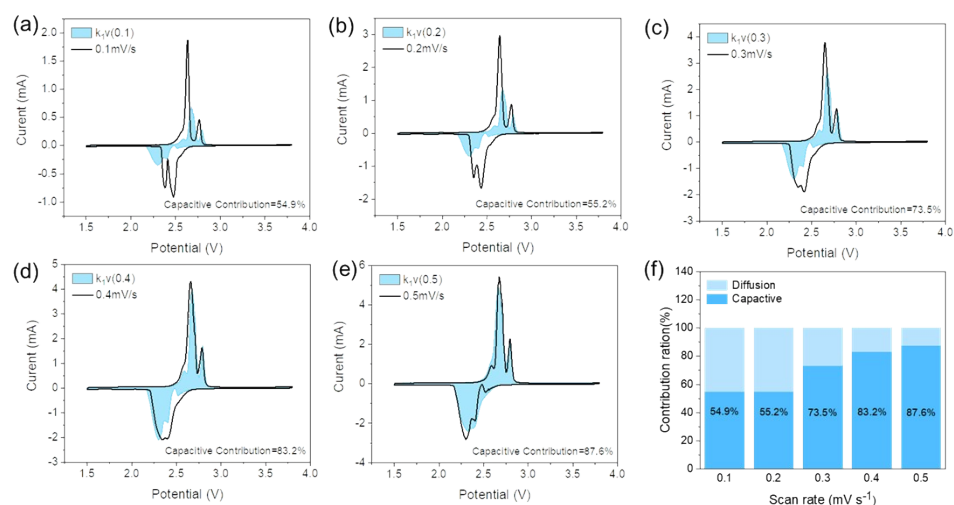


Fig. S4. CV curves and capacitive contributions of PDA cathode at scan rates of (a) 0.1, (b) 0.2, (c) 0.3, (d) 0.4, and (e) 0.5 mV s^{-1} ; (f) capacity contribution ratios of diffusion control and surface control at different scan rates.

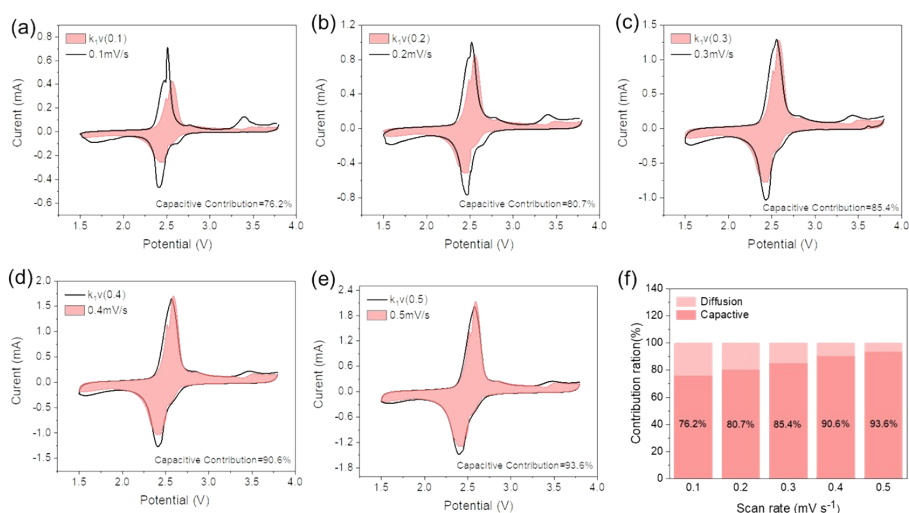


Fig. S5. CV curves and capacitive contributions of PDIN cathode at scan rates of (a) 0.1, (b) 0.2, (c) 0.3, (d) 0.4, and (e) 0.5 mV s⁻¹; (f) capacity contribution ratios of diffusion control and surface control at different scan rates.

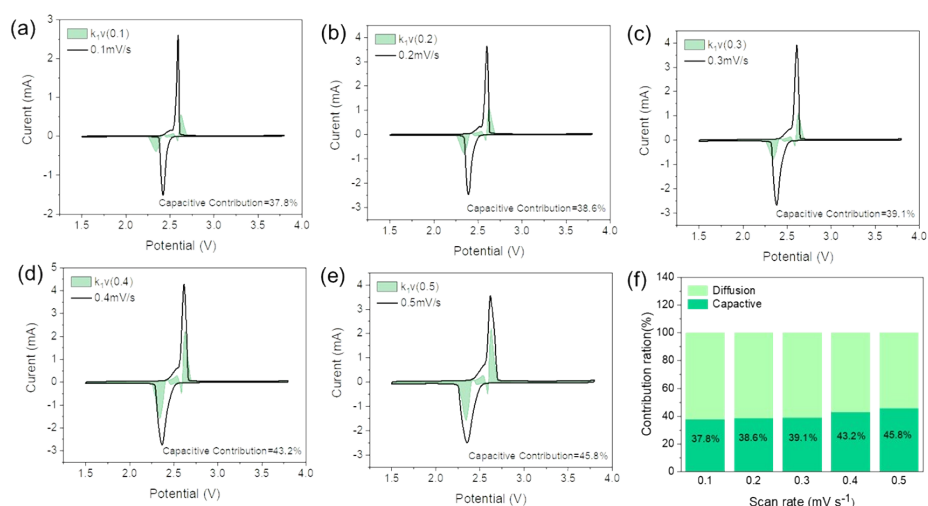


Fig. S6. CV curves and capacitive contributions of PDIC5 cathode at scan rates of (a) 0.1, (b) 0.2, (c) 0.3, (d) 0.4, and (e) 0.5 mV s⁻¹; (f) capacity contribution ratios of diffusion control and surface control at different scan rates.

Electrochemical impedance spectroscopy (EIS) measurements of the three molecules-based batteries after 5 cycles were conducted for further study, and the corresponding Nyquist plots are shown in Figure S7.² Compared with the PDA- and PDIC5-based batteries, the PDIN-based battery shows the smallest depressed semicircle at high to medium frequencies after 5 cycles, demonstrating the lowest charge transfer resistance (R_{ct}).³ The relative reduced R_{ct}

value contributes to rapid electrochemical kinetics, leading to enhanced rate performance and cycling stability of the PDIN-based battery.

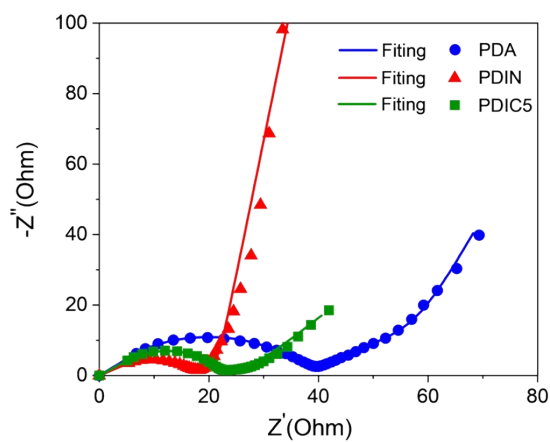


Fig. S7. Nyquist plots of PDA-, PDIN, and PDIC5-based batteries after 5 cycles.

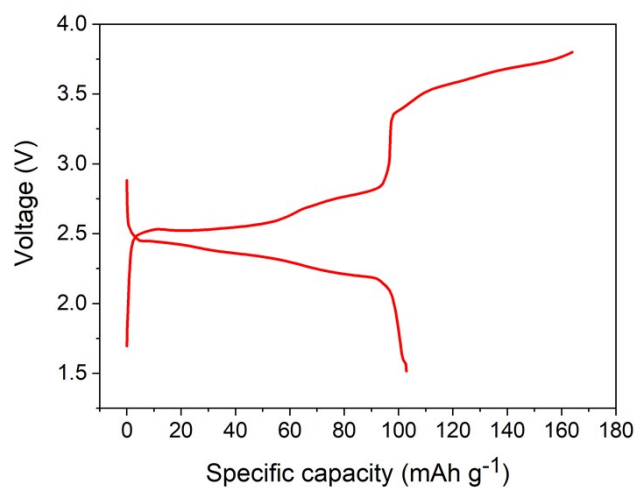


Fig. S8. The discharge/charge profiles in first cycle at 30 mA g⁻¹ of PDIN in the in situ FTIR measurement.

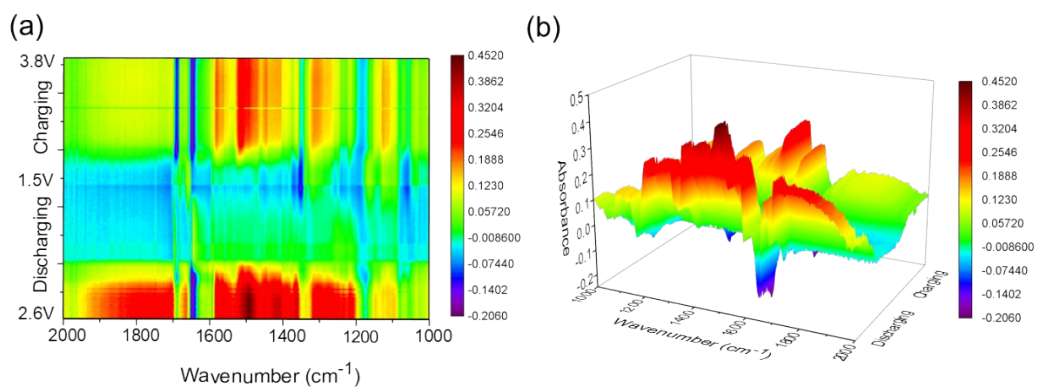


Fig. S9. 2D color-filled contour plot (a) and 3D diagram (b) of the in-situ FTIR test of PDIN-based battery under the first discharge/charge process.

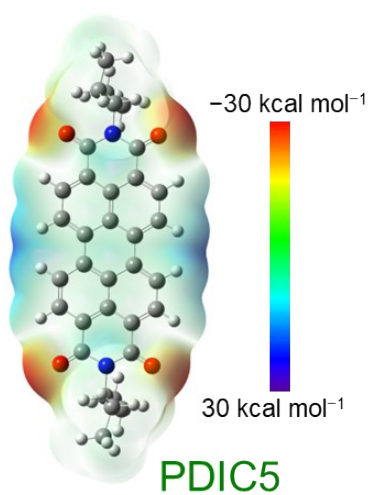


Fig. S10. MESP of PDIC5.

Table S1. DFT calculation results of PDA and PDIN (the C=O groups/Li reactions)^[a]

Calculation units	Free energy correction (a. u)	Single point energy (a. u)	Free energy (a. u)	Reactions	ΔG (a. u)	ΔG (kcal/mol)	ϕ vs Li ^{+/Li}
2Li	-0.01813	-15.0017	-15.0199				
PDA	0.2127	-1370.8291	-1370.6163				
PDA-2Li	0.2123	-1385.9976	-1385.7854	PDA + 2Li → PDA-2Li	-0.1492	-93.637	2.030
PDA-4Li	0.2101	-1401.0140	-1400.8039	PDA-2Li + 2Li → PDA-4Li	0.0013	0.804	-0.017
PDIN	0.5271	-1834.8497	-1834.3226				
PDIN-2Li	0.5339	-1850.0392	-1849.5053	PDIN + 2Li → PDIN-2Li	-0.1628	-102.186	2.215
PDIN-4Li	0.5306	-1865.0757	-1864.5451	PDIN-2Li + 2Li → PDIN-4Li	-0.02002	-12.563	0.272

^[a] The structures of these reactants and products were all optimized under the framework of density of functional theory (DFT) with m062x functional and def2-SVP basis set^{4,5}. The vibrational frequency analysis was carried out for the optimized structure with the same calculation method. The thermodynamic correction terms of the structures at 298.15 K were then obtained using Shermo program⁶. To obtain the electron energy with higher accuracy, the single point calculations for these optimized structures with m062x functional and def2-TZVP basis set were performed. Finally, the single point energy was added to the free energy correction calculated before to obtain the Gibbs free energy. All these DFT calculations were performed using Gaussian 16 program suite⁷. The molecular electrostatic potential surfaces (MESP) were calculated using Multiwfn program^{8,9} and then rendered using GaussView program.

References

- 1 Augustyn, V.; Come, J.; Lowe, M. A.; Kim, J. W.; Taberna, P. L.; Tolbert, S. H.; Abruña, H. D.; Simon, P.; Dunn, B. *Nature Materials*, 2013, **12**, 518-522.
- 2 Zhang, S. S.; Xu, K.; Jow, T. R. *Electrochimica Acta*, 2004, **49**, 1057-1061.
- 3 Qu, D. Y.; Wang, G. W.; Kafle, J.; Harris, J.; Crain, L.; Jin, Z. H.; Zheng, D. *Small Methods*, 2018, **2**, 1700342 .
- 4 Zhao, Y.; Truhlar, D. G. *Theoretical Chemistry Accounts*, 2008, **120**, 215-241.
- 5 Weigend, F.; Ahlrichs R. *Physical Chemistry Chemical Physics*, 2005, **7**, 3297-3305.
- 6 Lu, T.; Chen, Q. *Computational and Theoretical Chemistry*, 2021, **1200**, 113249.
- 7 Gaussian, Inc., Wallingford CT, 2016.
- 8 Lu, T.; Chen, F. *Journal of Molecular Graphics and Modelling*, 2012, **38**, 314-323.
- 9 Lu, T.; Chen, F. *Journal of Computational Chemistry*, 2012, **33**, 580-592.